JMEPEG (2007) 16:508–514
DOI: 10.1007/s11665-007-9066-7

1059-9495/$19.00

The Isothermal and Cyclic Oxidation Behavior of a Titanium Aluminide Alloy at Elevated Temperature

S.Y. Chang

(Submitted April 9, 2006)

The isothermal and cyclic oxidation behavior of Ti-47Al-2Mn-2Nb with 0.8 vol.% TiB_2 particle-reinforced alloy was investigated in air between 700 and 1000 °C. In the study, the kinetics of isothermal and cyclic oxidation were performed by using a continuous thermogravimetric method which permits mass change measurement under oxidation conditions. The oxide scales and substrates were characterized by scanning electron microscopy with energy-dispersive x-ray analysis and x-ray diffraction. At 700 and 800 °C, the alloy showed an excellent oxidation resistance under isothermal and cyclic conditions. After exposure to air above 800 °C, the outer scale of the alloy was dominated by a fast-growing TiO_2 layer. Under the coarse-grained TiO_2 layer was the Al_2O_3-rich scale, which was fine-grained. At 900 and 1000 °C, the extent of oxidation increased clearly. The oxidation rate follows a parabolic law at 700 and 800 °C. However, the alloy, upon isothermal oxidation at 900 °C, can be divided into several stages. During the cyclic oxidation at 900 and 1000 °C, partial scale spallation takes place, leading to a stepwise mass change.

Keywords cyclic oxidation, isothermal oxidation, oxidation kinetics, thermogravimetric analysis, TiAl-based intermetallic

1. Introduction

TiAl intermetallic compounds have potential aerospace and automotive engine applications because of their rather high-temperature creep resistance, good oxidation resistance, high stiffness at high temperature, and low density (ca. 3.8 g/cm^3) (Ref 1-3). However, the use of titanium aluminides has been limited by relatively poor oxidation resistance at elevated temperatures and inherent poor formability and embrittlement at low temperatures. One possibility to improve the room temperature ductility of γ-TiAl alloy is given by the addition of manganese or vanadium elements. The addition of TiB_2 particles can effectively enhance the mechanical properties of γ-TiAl alloys (Ref 4). Despite their high aluminum content, TiAl-based alloys do not easily form long-lasting protective alumina scales during oxidation at temperatures of beyond 700 °C (Ref 5-8). It has been demonstrated that small additions of Nb, Cr, or Si to the γ-TiAl-based intermetallic alloys can improve the oxidation resistance (Ref 9-14). The aim of the present study is to characterize the isothermal and cyclic oxidation behavior of the Ti-47Al-2Mn-2Nb + 0.8 vol.% TiB_2 alloy over a wide temperature range of 700-1000 °C in air. Thermogravimetric analysis was used to determine the oxidation kinetics and to monitor the occurrence of oxide scale cracking and spalling. X-ray diffraction (XRD), scanning electron microscopy (SEM), and energy-dispersive x-ray analysis (EDX) were used to establish the composition and structure of the scales. In this study, the oxidation mechanism of this alloy is also discussed.

S.Y. Chang, Department of Mechanical Engineering, National Yunlin University of Science & Technology, 640 Touliu, Taiwan. Contact e-mail: changsy@yuntech.edu.tw.

2. Experimental Procedures

The chemical compositions of the TiAl alloy investigated are given in Table 1. The material was obtained by vacuum melting and casted in the form of cylindrical bars with a diameter of 15 mm. In order to obtain a homogenous microstructure, this material was subsequently annealed in vacuum at 1010 °C for 50 h.

Disk samples about 1 mm thick were cut from the received rods using a low-speed saw. The specimens were wet ground with SiC paper to 1200 grit and then polished with a 1 μm diamond suspension on all faces. Before the oxidation tests, the specimens were cleaned with acetone in an ultrasonic bath for 5 min and dried in air. Isothermal and cyclic oxidation was performed at 700-1000 °C in static laboratory air using a thermomicrobalance with a sensitivity of 1 μg. Each sample was inserted in the furnace to heat while the temperature reached the oxidation temperature. A computer-controlled device was used to periodically move the specimens into and out of the hot zone of the furnace. Insertion and removal of the specimens were carried out in a few seconds to guarantee rapid heating and cooling. The period of cyclic oxidation was 1 or 5 h at reaction temperature, and 15 min at ambient temperature, which appeared to be long enough to cool the specimens from 1000 °C to below 50 °C. The temperature profile during the two cycles for 1 h cyclic oxidation at 1000 °C is given in Fig. 1. In order to observe the oxide structure, isothermal oxidation tests were also conducted in a furnace with varied testing times from 3 to 200 h. After the specified periods, the specimens were cooled in the furnace.

The composition, the phases, and the morphology of the oxidation products formed in external scales and in subsurface regions were investigated using optical microscopy, SEM equipped with an EDX, and XRD.

3. Results and Discussion

The mass change per unit surface area versus the exposure time under isothermal oxidation in the continuous thermogravimetric measurements at 700-1000 °C in air are shown in Fig. 2. The thermogravimetric studies showed that the oxidation rate increased with oxidation temperature. The oxidation curves show relatively slow mass gains at 700 and 800 °C. The mass gains upon 100 h of exposure time at 700 and 800 °C are rather small, but the mass gain increases rapidly at 900 and 1000 °C. There are two different stages in the kinetics during isothermal oxidation at 900 °C exposure to air. In the initial oxidation stage was evident a more rapid oxidation. After 22 h of oxidation, a more protective behavior against isothermal oxidation was found, and a lower oxidation rate was exhibited. The mass change curve showed that the alloy, during isothermal oxidation at 1000 °C, could be divided into several stages. At that temperature, the oxidation process represents the initial stage with a very high oxidation rate. In order to indicate whether any laws of kinetics apply, the oxidation curves were expressed in a log-log plot, shown in Fig. 3.

During the oxidation periods, the slopes of all the curves in Fig. 3 are close to 0.5, indicating that the oxidation is nearly parabolic. Figure 4 is the parabolic kinetics plot of the samples from Fig. 2. The linear portion of each of these plots represents the behavior of parabolic oxidation at the corresponding temperatures. Despite the deviation for the 1000 °C curve,

Table 1 Chemical composition of the TiAl alloy tested

	Ti	Al	Mn	Nb	B	Si	Fe	Cu	O	N	H
at.%	Rest	46.57	2.01	2.04	1.15	0.06	0.034	0.03	0.123	0.021	0.019

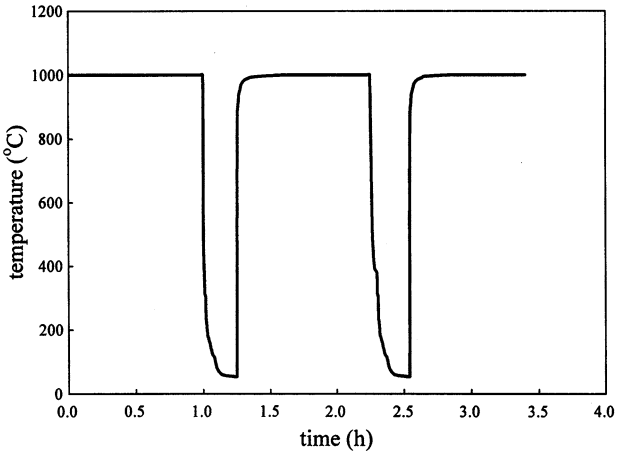

Fig. 1 Temperature time profile for two cycles for 1-h cyclic oxidation with an upper temperature of 1000 °C

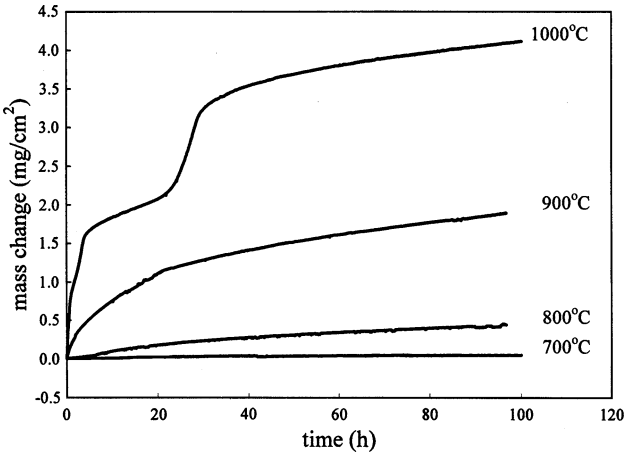

Fig. 2 Mass change as a function of time for the oxidation of the TiAl alloy at various temperatures

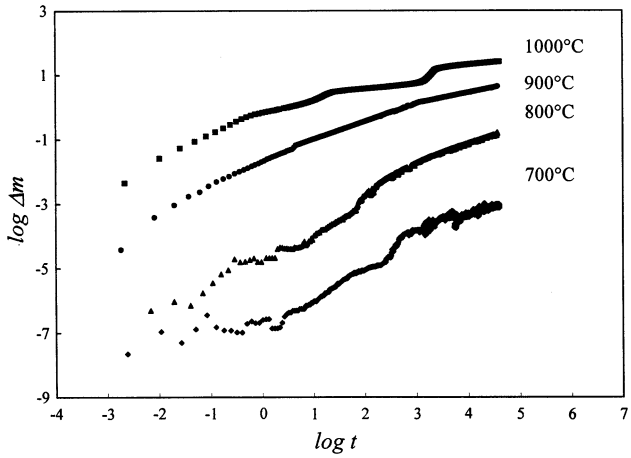

Fig. 3 Log-log plots of oxidation curves

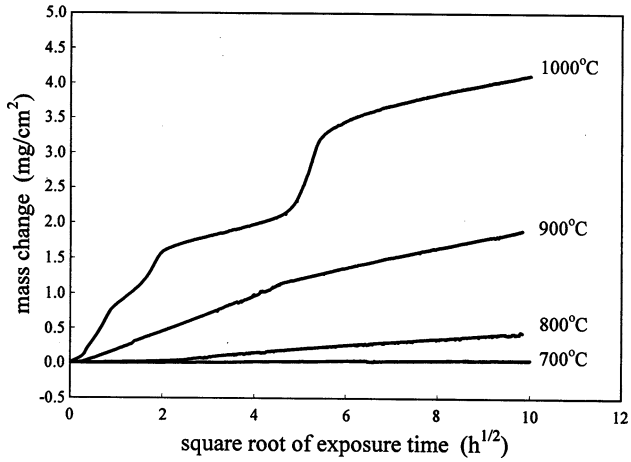

Fig. 4 Parabolic kinetic plots of oxidation curves

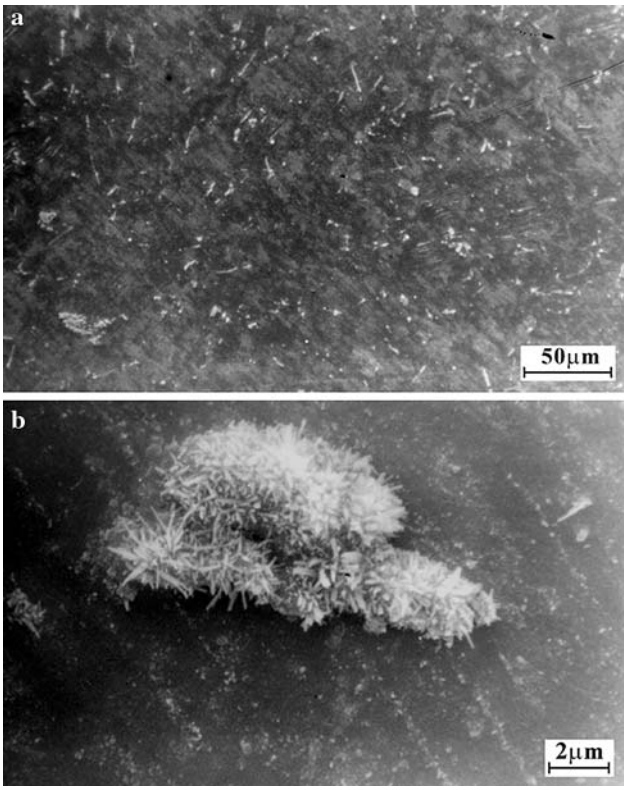

Fig. 5 SEM surface morphology of TiAl alloy after exposure to air at 700 °C for 150 h

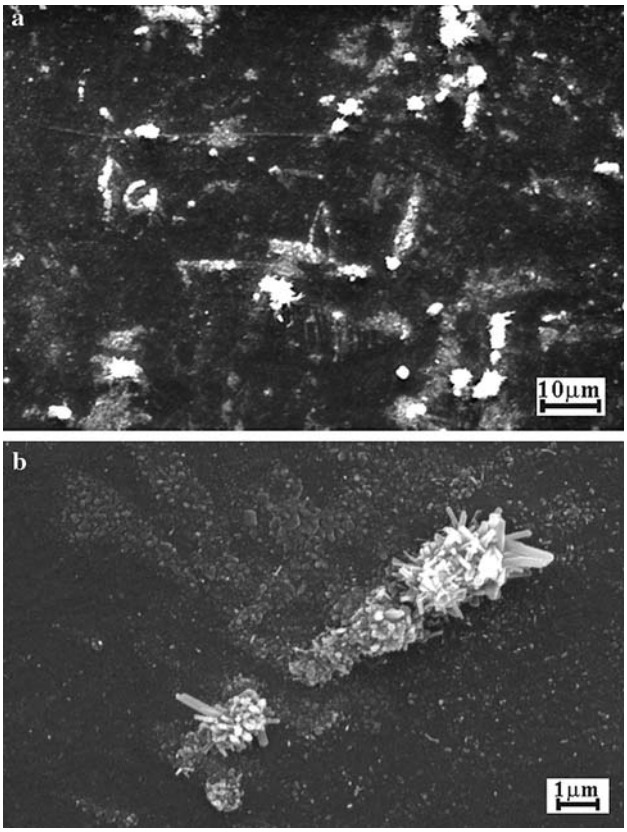

Fig. 6 SEM surface morphology of TiAl alloy after exposure to air at 700 °C for 200 h

the oxidation rates for different stages could be described by parabolic kinetics. Thus, the results indicate that the isothermal oxidation rate of the TiAl alloy is diffusion controlled (Ref 15). Both periods of the isothermal oxidation at 900 °C could be described by parabolic kinetics, with a parabolic rate constant ($k_p = \Delta m/t^{1/2}$) of approximately 0.062 mg cm^{-2} $h^{-0.5}$ for the first stage, whereas that for the second stage was 0.05 mg cm^{-2} $h^{-0.5}$. The parabolic rate constants for the isothermal oxidation at 700 and 800 °C are 0.0048 and 0.043 mg cm^{-2} $h^{-0.5}$, respectively.

The surface morphology after 150 and 200 h isothermal oxidation at 700 °C is shown in Fig. 5(a) and 6(a). After oxidation at 700 °C, no clear and homogenous oxide scale was found. Some areas revealed several small needlelike crystals, as

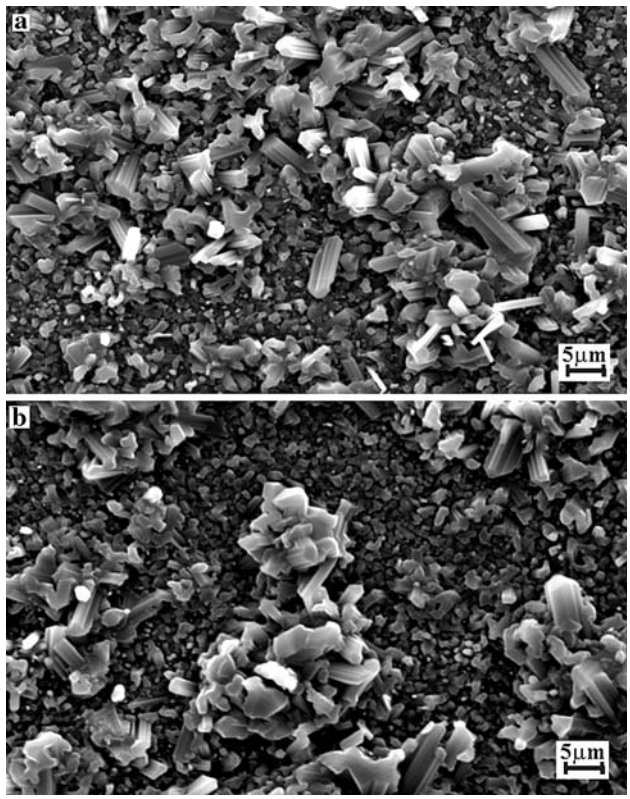

Fig. 7 SEM surface morphology of TiAl alloy after exposure to air at 800 °C for (a) 100 h and (b) 200 h

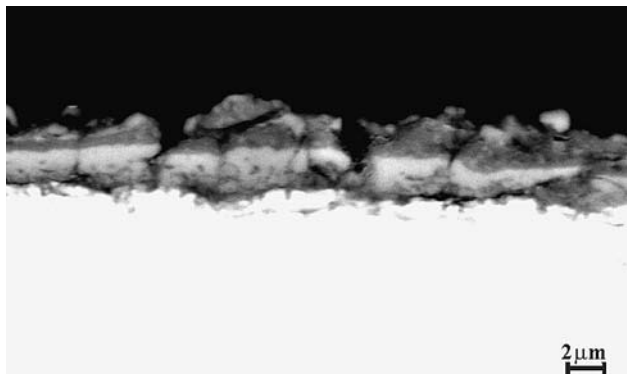

Fig. 8 Cross-sectional SEM micrograph of TiAl alloy after exposure to air at 800 °C for 200 h

shown in Fig. 5(b) and 6(b), which were determined to be rich in titanium and oxygen by EDX tests. After 100 h of exposure at 800 °C, the surface of the alloy was covered with small oxide grains. A thin oxidation layer had formed. EDX tests indicated that the outer layer of the scale consists predominantly of titanium and oxygen. Figure 7 shows the surface morphology of the alloy after 100 and 200 h of isothermal oxidation at 800 °C. No spallation of oxide particles was observed after cooling. A metallographic cross section of the alloy after 200 h of exposure to air at 800 °C is shown in Fig. 8. The thickness of the oxide scale was approximately 2.5 μm.

The surface morphology of the alloy oxidized for different exposure times at 900 °C is shown in Fig. 9. Rutile crystals of the outer layer become large when the oxidation temperature exceeded 900 °C. With the increase in exposure time came increases in the size of the oxide crystals. The oxide scale had partially spalled after cooling. It can be observed that the outer part of the non-spalled surface scale consisted of an outer layer of a coarse-grained oxide and an inner part of a more fine-grained structure, as shown in Fig. 10. EDX elemental mapping of the oxide scale revealed that the outer layer was rich in titanium. Under the outer layer was a layer rich in aluminum.

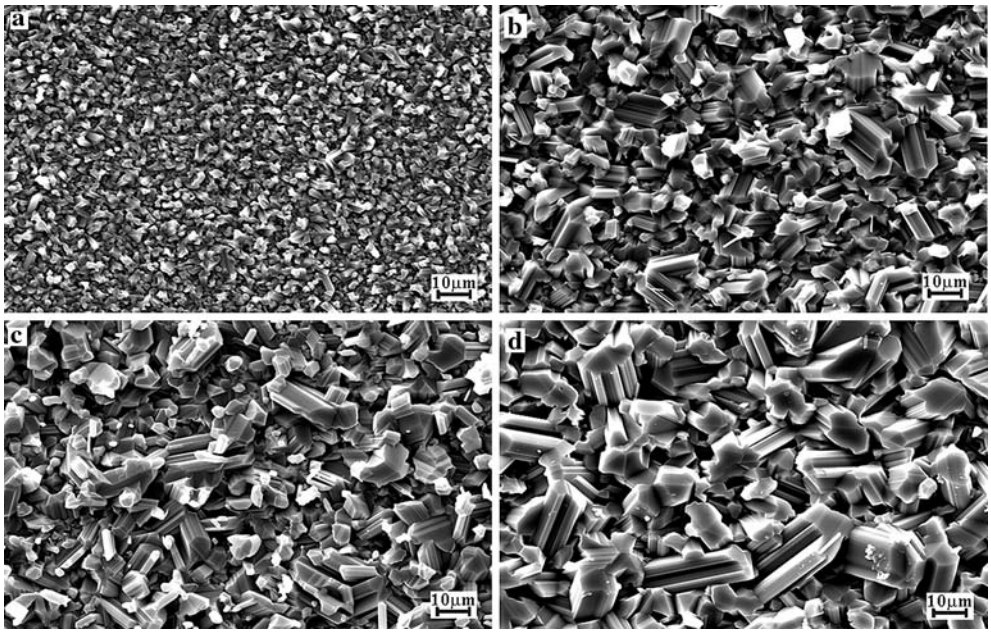

Fig. 9 SEM surface morphology of TiAl alloy after exposure to air at 900 °C for (a) 3 h, (b) 50 h, (c) 100 h, and (d) 150 h

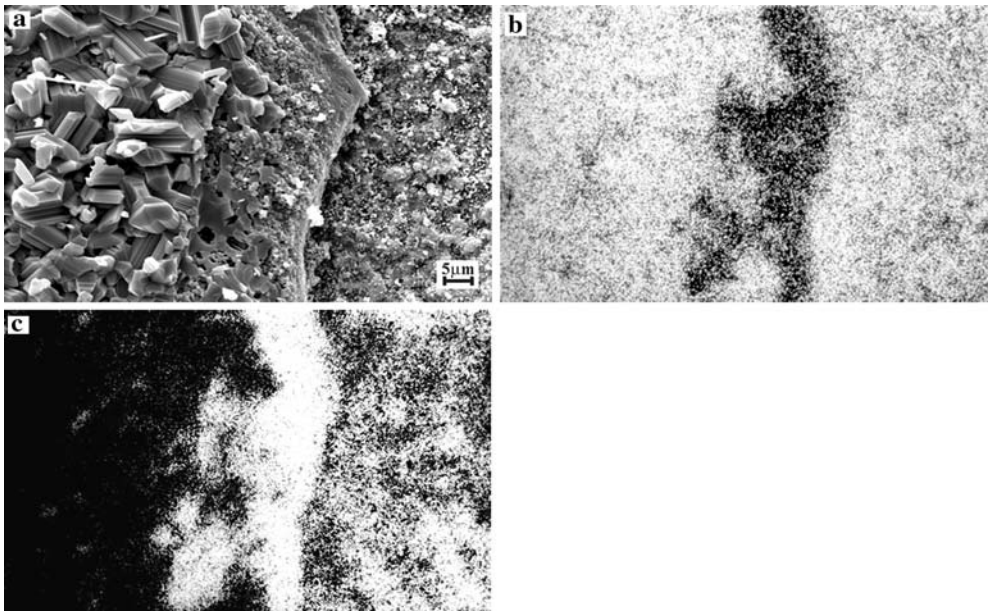

Fig. 10 Micrograph and EDX analyses of TiAl alloy after exposure to air at 900 °C for 150 h: (a) SEM micrographs; (b) and (c) elemental mapping of Ti and Al, respectively

The inner part showed a fine-grained structure containing both titanium and aluminum. At 900 °C, after an exposure time of about 20 h, the oxidation rate decreased. That is indicative of the formation of a relatively protective oxide scale after oxidation for 20 h. In the second stage, the oxidation rate is comparable to alumina formers. Figure 11 shows SEM micrographs of the surface morphology of the alloy oxidized for 3, 20, and 100 h at 1000 °C. Long-term exposure of the alloy to air increases the size of the oxide crystals. At this temperature, the sample showed significant spallation of the oxide scale after cooling. EDX analysis of the oxide scale revealed results that were similar to those for the alloy oxidized at 900 °C.

A significantly high oxidation rate was found at 1000 °C at the initial stage of the isothermal oxidation process, as shown in Fig. 2. After an exposure time of about 2 h, a protective oxide scale had formed, which resulted in a marked decrease of the oxidation rate. After that stage (about 5 h of oxidation), a transition to a more rapid oxidation rate was observed. This stage was characterized by a loss of the protectivity of the scales formed. In the last stage, the protective oxide scale formed again. The kinetics of Ti oxide formation are typically greater than those of Al_2O_3 formation. Consequently, the metal surface was rapidly covered with a thin layer of Ti oxide. This led to a local enrichment of the intermetallic in Al below the oxide surface, locally changing the stoichiometry, which favors the formation of Al_2O_3.

The influence of temperature on the cyclic oxidation behavior is summarized in Fig. 12. Under cyclic oxidation conditions, the alloy that showed at 700 and 800 °C a similar parabolic oxidation behavior was found under isothermal conditions. No measurable mass loss was found for cyclic testing at 700 and 800 °C, which is an indication of good

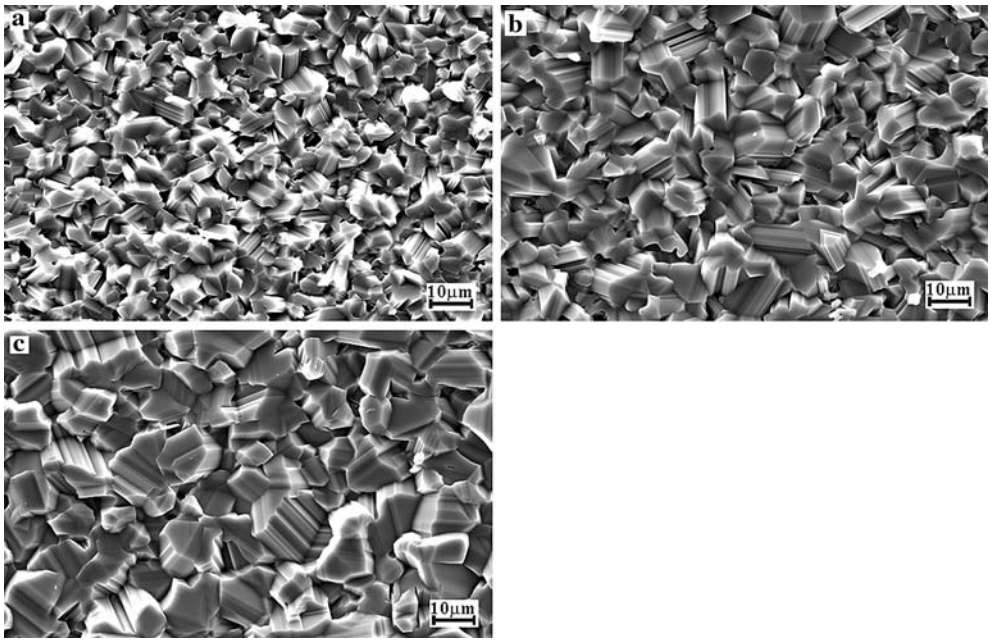

Fig. 11 SEM surface morphology of TiAl alloy after exposure to air at 1000 °C for (a) 3 h, (b) 20 h, and (c) 100 h

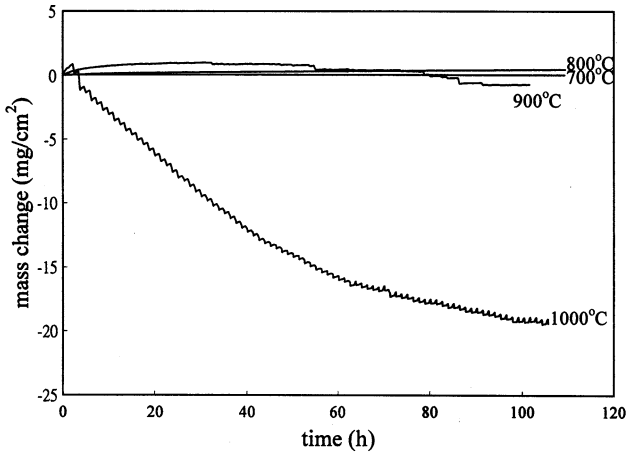

Fig. 12 Mass change as a function of time for the cyclic oxidation of the TiAl alloy at various temperatures

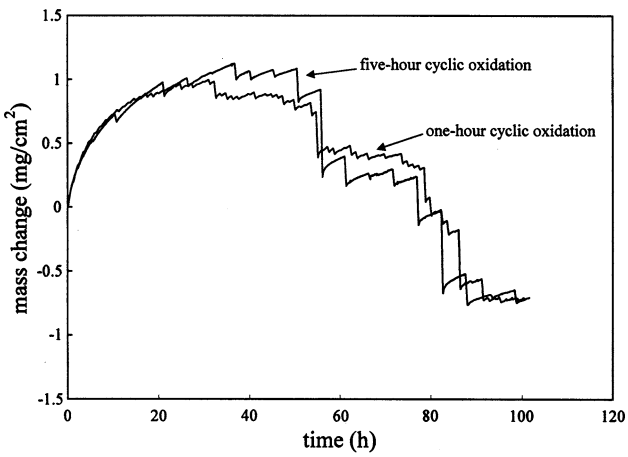

Fig. 13 Mass change as a function of time for the 1-h and 5-h cyclic oxidation at 900 °C

resistance against cyclic oxidation under the temperatures. The surface morphology of the alloy after 100 h of cyclic oxidation at 700 and 800 °C was also similar to that observed after isothermal oxidation. A stepwise spalling of the oxide scale at 900 and 1000 °C was observed. Figure 13 shows the mass change as a function of time for the 1 and 5-h cyclic oxidation at 900 °C. During the initial period of the cyclic oxidation for both conditions at 900 °C, only slightly spallation can be observed. After about 50 h of cyclic oxidation, mass loss clearly occurred. In contrast to the weight change behavior under 900 °C cyclic oxidation, the scale spalled disastrously, causing a massive weight loss for cyclic testing at 1000 °C, as shown in Fig. 14. During cyclic oxidation tests performed at 1000 °C, the alloy showed the rapid formation of an oxide scale following the periodic oxide spalling. Figure 2 shows rapid oxidation in the initial oxidation stage of isothermal oxidation at 1000 °C. Up to about 2 h of oxidation, a more protective oxide scale can form and exhibits a lower oxidation rate. Thus, in contrast to the weight change behavior, under 1 and 5-h cyclic oxidation at 1000 °C showed the 1 h cyclic oxidation causing a larger weight loss.

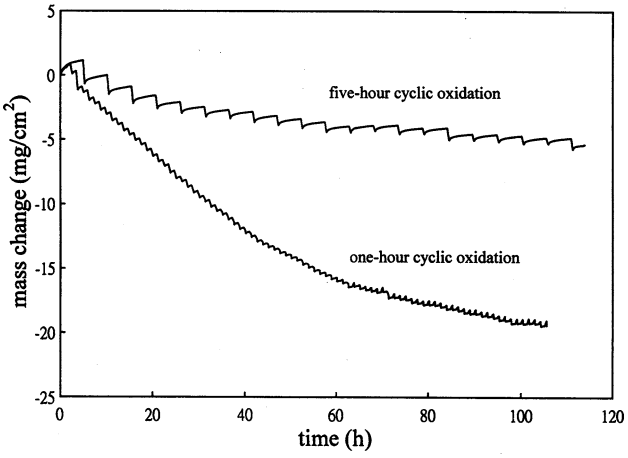

Fig. 14 Mass change as a function of time for the 1-h and 5-h cyclic oxidation at 1000 °C

After 100 h of cyclic oxidation at 900 and 1000 °C, a lamella oxide layer was observed, which is presented in Fig. 15 and 16. The scale surface in unspalled areas revealed large crystals of TiO_2, the same morphology as that after isothermal oxidation. During cyclic oxidation, spalling and forming of the oxide scale takes place. The microstructure of the oxide scale consisted of the lamellar structure of a coarse-grained Ti-rich oxide and fine-grained Al-rich oxide and showed that the layers had about the same thickness. Figure 17 is the EDX element mapping of the cross section of specimens after cyclic oxidation for 100 h at 1000 °C. The outer part of each oxide scale contains mainly titanium (the brighter parts in Fig. 16a). Inner oxide scales were determined to be rich in aluminum (the darker parts in Fig 16a). Under the defined cyclic oxidation conditions at all temperatures, internal oxidation has not been observed.

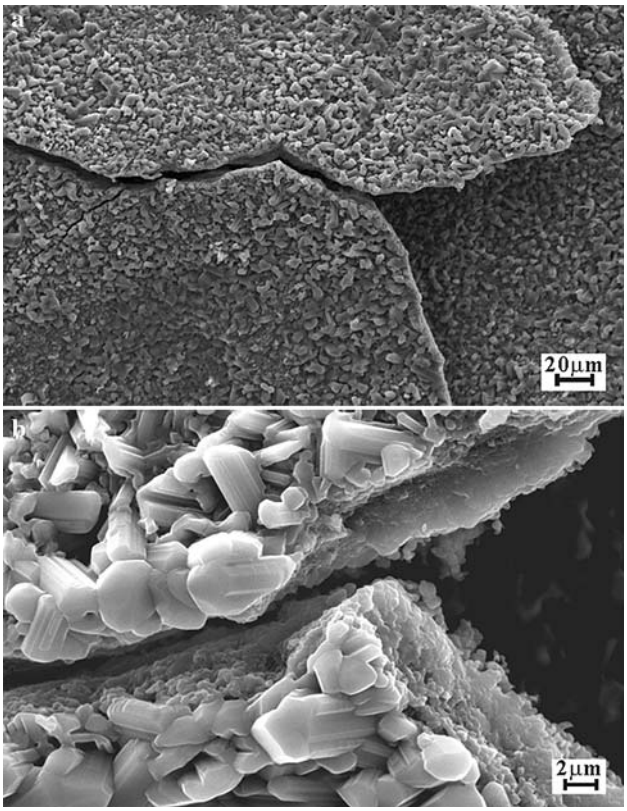

Fig. 15 SEM Micrograph of TiAl alloy after 5-h cyclic oxidation at 900 °C for 100 h

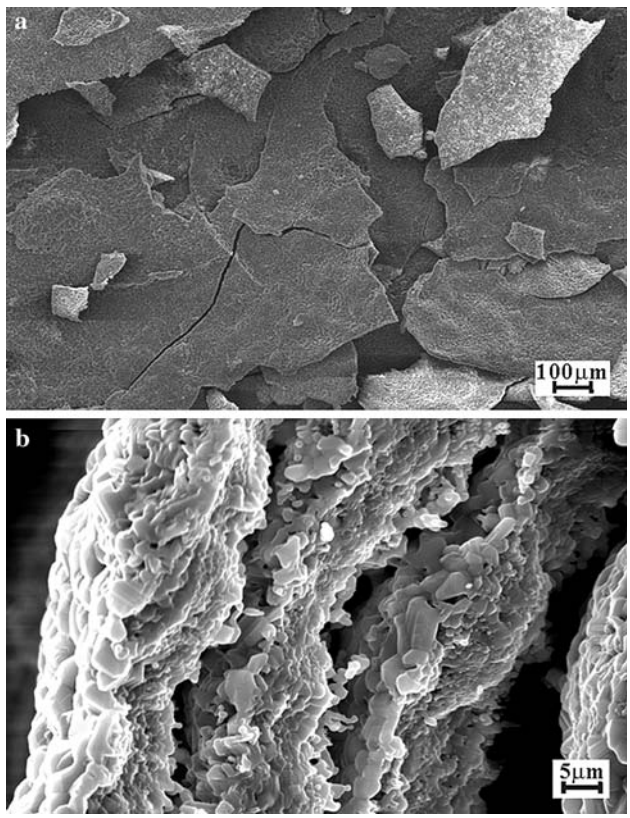

Fig. 16 SEM Micrograph of TiAl alloy after cyclic oxidation at 1000 °C for 100 h

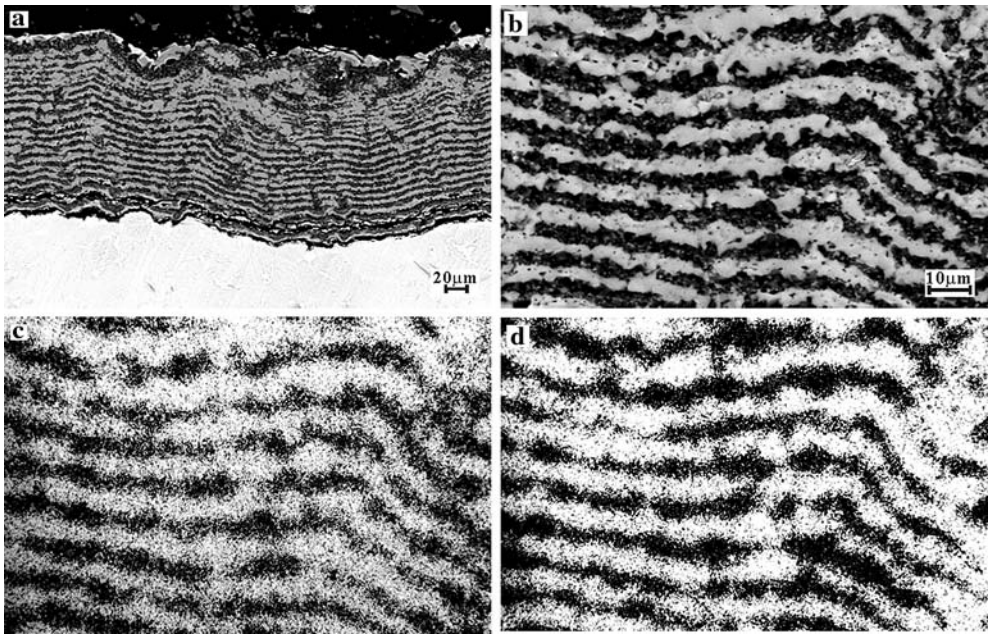

Fig. 17 Micrograph and EDX analyses of oxide scale on TiAl alloy after cyclic oxidation at 1000 °C for 100 h: (a) and (b) cross-sectional SEM micrograph SEM micrographs; (c) and (d) elemental mapping of Ti and Al for (b), respectively

4. Conclusions

At 700 and 800 °C, the intermetallic alloy showed an excellent resistance against isothermal and cyclic oxidation in air. No major differences were found in microstructure and composition between the oxides formed under isothermal and cyclic oxidation at 700 and 800 °C. The behavior of oxidation in all cases studied at 700-1000 °C followed a parabolic relationship. A strong influence of the temperature on the oxidation rate was observed. The oxidation process at 900 and 1000 °C can be divided into several stages. The cyclic oxidation resistance of the alloy was poor due to the spalling of the oxide layer at 900 and 1000 °C. Under cyclic oxidation at 900 and 1000 °C, the oxide scales showed significant cracking and spallation. This process led to a stratified scale. In general, the microstructure of the oxide scale is an outer scale of fast-growing TiO_2 and an internal scale of Al_2O_3. However, since Al_2O_3 does not form a continuous barrier, generally, the scale is non-protective beyond 800 °C.

Acknowledgment

Special thanks go to National Science Council (under Grant# NSC94-2216-E-010-CC3) for their sponsorship of this research project.

References

1. P.R. Subramanian, M.G. Mendiratta, D.M. Dimiduk, and M.A. Stucke, Advanced Intermetallic Alloys—Beyond Gamma Titanium Aluminides, *Mater. Sci. Eng. A*, 1997, **A239-A240**, p 1–13
2. E.A. Loria, Gamma Titanium Aluminides as Prospective Structural Materials, *Intermetallics*, 2000, **8**, p 1339–1345
3. T. Tetsui, Gamma Ti Aluminides for Non-Aerospace Applications, *Curr. Opin. Solid State Mater Sci.*, 1999, **4**, p 243–248
4. R.A. Mirshams, Z.X. Li, and H.P. Mohamadian, High-Temperature Tensile Properties and Fracture Characteristics in a Monolithic Gamma TiAl Alloy and a TiB_2 Particle-Reinforced TiAl Alloy, *J. Mater. Sci. Lett.*, 1997, **16**, p 715–718
5. V.A.C. Haanappel, R. Hofman, J.D. Sunderkötter, W. Glatz, H. Clemens, and M.F. Stroosnijder, The Influence of Microstructure on the Isothermal and Cyclic-Oxidation Behavior of Ti-48Al-2Cr at 800 °C, *Oxidation Met*, 1998, **48**(3-4), p 263–287
6. G. Schumacher, F. Detteneanger, M. Schütze, U. Hornauer, E. Richter, E. Wieser, and W. Möller, Microalloying Effects in the Oxidation of TiAl Materials, *Intermetallics*, 1999, **7**, p 1113–1120
7. V.A.C. Haanappel, W. Glatz, H. Clemens, and M.F. Stroosnijder, The Isothermal and Cyclic Oxidation Behaviour of Ti-48Al-2Cr at 700°C, *Mater. High Temperatures*, 1997, **14**(1), p 19–25
8. S. Becker, M. Schütze, and A. Rahmel, Cyclic Oxidation Behaviour of TiAl and of TiAl Alloys, *Oxidation Met*, 1993, **39**(1/2), p 93–106
9. M. Yoshihara and K. Miura, Effects of Nb Addition on Oxidation Behavior of TiAl, *Intermetallics*, 1995, **3**, p 357–363
10. S. Taniguchi, K. Uesaki, Y.-C. Zhu, Y. Matsumoto, and T. Shibata, Influence of Implantation of Al, Si, Cr or Mo Ions on the Oxidation Behaviour of TiAl Under Thermal Cycle Conditions, *Mater. Sci. Eng. A*, 1999, **A266**, p 267–275
11. B.G. Kim, G.M. Kim, and C.J. Kim, Oxidation Behavior of TiAl-X (X=Cr, V, Si, Mo or Nb) Intermetallics at Elevated Temperature, *Scr Metall Mater*, 1995, **33**(7), p 1117–1125
12. V.A.C. Haanappel, J.D. Sunderkötter, and M.F. Stroosnijder, The Isothermal and Cyclic High Temperature Oxidation Behaviour of Ti-48Al-2Mn-2Nb Compared with Ti-48Al-2Cr-2Nb and Ti-48Al-2Cr, *Intermetallics*, 1999, **7**, p 529–541
13. Y. Wu, K. Hagihara, and Y. Umakoshi, Improvement of Cyclic Oxidation Resistance of Y-containing TiAl-based Alloys with Equiaxial Gamma Microstructures, *Intermetallics*, 2005, **13**, p 879–884
14. J.D. Sunderkötter, H.J. Schmutzler, V.A.C. Haanappel, R. Hofman, W. Glatz, H. Clemens, and M.F. Stroosnijder, The High-Temperature Oxidation Behaviour of Ti-47Al-2Cr-0.2Si and Ti-48Al-2Cr-2Nb Compared with Ti-48Al-2Cr, *Intermetallics*, 1997, **5**, p 525–534
15. S.A. Kekare and P.B. Aswath, Oxidation of TiAl Based Intermetallics, *J. Mater. Sci.*, 1997, **32**, p 2485–2499